Monthly Notices
of the
ROYAL ASTRONOMICAL SOCIETY

MNRAS **467,** 2585–2593 (2017) doi:10.1093/mnras/stx225
Advance Access publication 2017 January 27

A numerical investigation of wind accretion in persistent supergiant X-ray binaries – I. Structure of the flow at the orbital scale

I. El Mellah★ and F. Casse

APC AstroParticule and Cosmology laboratory – Université Paris 7 Diderot Sorbonne Paris Cité, 10 rue Alice Domon et Léonie Duquet, F-75013 Paris, France

Accepted 2017 January 23. Received 2017 January 16; in original form 2016 August 4

ABSTRACT

Classical supergiant X-ray binaries host a neutron star orbiting a supergiant OB star and display persistent X-ray luminosities of 10^{35}–10^{37} erg s^{-1}. The stellar wind from the massive companion is believed to be the main source of matter accreted by the compact object. With this first paper, we introduce a ballistic model to evaluate the influence of the orbital effects on the structure of the accelerating winds that participate to the accretion process. Thanks to the parametrization we retained the numerical pipeline we designed, we can investigate the supersonic flow and the subsequent observables as a function of a reduced set of characteristic numbers and scales. We show that the shape of the permanent flow is entirely determined by the mass ratio, the filling factor, the Eddington factor and the α-force multiplier that drives the stellar wind acceleration. Provided scales such as the orbital period are known, we can trace back the observables to evaluate the mass accretion rates, the accretion mechanism, the shearing of the inflow and the stellar parameters. We discuss the likelihood of wind-formed accretion discs around the accretors in each case and confront our model to three persistent supergiant X-ray binaries (Vela X-1, IGR J18027−2016, XTE J1855−026).

Key words: accretion, accretion discs – stars: massive – stars: neutron – stars: winds, outflows – X-rays: binaries.

1 INTRODUCTION

For the last 50 yr, X-ray observations have revealed a plethora of binary systems hosting a compact object accreting the gas from its stellar companion. In high-mass X-ray binaries (HMXB), the dense and fast winds of massive stars – which generally do not fill their Roche lobe – is expected to be the main responsible for mass transfer. The structure of the wind in HMXB has been found to be of two kinds (Chaty 2011): either it forms a circumstellar decretion disc around fast rotators Be stars (BeXB) or it obeys the more isotropic sketch of the radiatively driven wind for early-type supergiant stars (Shakura et al. 2015). The latter sources of matter are believed to be associated with the class of the persistent classical supergiant X-ray binaries (SGXB) when surrounded by a neutron star on a low-eccentricity orbit thus making the compact object permanently embedded in the wind. The number of confirmed SGXB has doubled within the last 10 years (Walter et al. 2015) which makes it possible to significantly discard or confirm correlations between their intern parameters such as the spin period, the orbital period or the X-ray luminosity. In spite of the high intrinsic absorption in those systems (Filliatre & Chaty 2004), thorough observations have shed light on the nature of the donor star (Coleiro & Chaty 2013) and of its wind (Gimenez-Garcia et al. 2016).

The theory of radiatively driven winds (or CAK winds) for isolated massive stars has been widely developed, refined and confronted to observations since the seminal papers of the 1970s (Lucy & Solomon 1970; Castor, Abbott & Klein 1975). It describes how the resonant absorption of the high energy photons of hot stars by non-fully ionized metals supplies the outer layers with net linear momentum. As they accelerate, they keep absorbing Doppler shifted photons previously untouched (Kudritzki & Puls 2000; Puls, Vink & Najarro 2008). Because of the existence of a critical permanent solution in this model, the wind properties are entirely determined by the stellar parameters and a few force multipliers set by the thermochemical properties of the atmosphere. The latter have been precisely computed, in particular, in the case of supergiant stars (Crowther, Lennon & Walborn 2006) of spectral type similar to the donor stars in SGXB.

In this paper, we build a model to empirically couple the stellar, orbital, wind and accretion properties in SGXB hosting a confirmed neutron star. Because of the high mass ratio in these systems, we do not expect the launching of the wind to be significantly altered by the presence of the neutron star; yet, the non-inertial forces at stake in those relatively short periods systems (<20 d) will modify the structure of the departed though still accelerating flow as it

★ E-mail: ileyk@apc.univ-paris7.fr

approaches the compact object, where the gravitational field of the latter will take over. Concerned with the permanent behaviour of classical SGXB, we focus on the self-consistent trends that arise between coupled quantities we do not force, such as the spectral type of the donor and the X-ray luminosity of the system. In particular, we identify the fundamental parameters favourable to the formation of a wind capture disc so as to make possible in a following paper targeted simulations of the hydrodynamical behaviour of the flow for configurations of interest. Radiatively driven winds are notoriously unstable to small-scale radial perturbations (MacGregor, Hartmann & Raymond 1979; Owocki & Rybicki 1984, 1985); but to disentangle between the time variability induced by clumps in the feeding wind (Ducci et al. 2009), X-ray ionizing feedback (Ho & Arons 1987a; Blondin et al. 1990; Manousakis & Walter 2015), disc instabilities (Foulkes, Haswell & Murray 2006) or other phenomena (Illarionov & Sunyaev 1975; Shakura, Postnov & Hjalmarsdotter 2013), we must wonder about the conditions to form a disc out of a permanent inflow. This question has been successfully handled for binary systems where a star or a white dwarf accretes the matter from its asymptotic giant branch companion (Theuns & Jorissen 1993; Theuns, Boffin & Jorissen 1996; Jahanara et al. 2005; Mohamed & Podsiadlowski 2007; de Val-Borro, Karovska & Sasselov 2009; Huarte-Espinosa et al. 2013); the winds of those stars are however much slower than the radiatively driven wind of supergiant stars, which makes the disc formation not obvious in SGXB.

We set the modelling stage of our toy model in Section 2 and highlight its fundamental parameters. After a description of our numerical pipeline in Section 3, we discuss the structure of the flow at the orbital scale and its properties (mass accretion rate on to the compact object and shearing of the flow) in Section 4. Finally, we summarize our results, confront them with three extensively studied classical SGXB (Vela X-1, XTE J1855−026 and IGR J18027−2016) and discuss the main implications of this model in Section 5.

2 RADIATIVELY DRIVEN WIND IN A SGXB ROCHE POTENTIAL

2.1 Radiatively driven winds of hot stars

2.1.1 The bedrock model

In addition to the radiative pressure due to Thomson scattering of light on the free electrons in stellar atmospheres, spectral lines of partly ionized metals can induce a resonant absorption of the high energy photons provided by hot stars (see e.g. Lamers & Cassinelli 1999). The underlying radiations tend to produce a net acceleration of those ions in the same direction, as they isotropically re-emit the absorbed photons from below.[1] Through Coulomb coupling of those metal ions with the ambient charged particles, momentum is redistributed and the whole gas is lifted up from the outer layers of the star. As the radial velocity rises, Doppler shifting of the absorption lines enables the metal ions to keep tapping radiative energy. Under additional assumptions concerning the spectral and spatial narrowness of the absorption process (the Sobolev approximation) and if we reduce the emission region to a point, one can write the corresponding acceleration term as (Castor et al. 1975):

$$g_{\rm CAK} = \frac{Q}{1-\alpha}\frac{\kappa_{\rm e} L_*}{4\pi r^2 c}\left(\frac{1}{\rho c \kappa_{\rm e} Q}\frac{{\rm d}v}{{\rm d}r}\right)^{\alpha}. \quad (1)$$

[1] In the single scattering limit.

One recognizes a contribution analogous to the radiative acceleration due to the continuum opacity by electron scattering (the second factor on the right-hand side), with $\kappa_{\rm e}$ being the free electrons opacity, L_* the stellar luminosity, c the speed of light and r the distance to the stellar centre. The α and Q factors are the two dimensionless force multipliers, the fundamental parameters that structure the form and the amplitude of the physical quantities of the flow. The former stands for the relative contribution of thin and thick absorption lines to the net acceleration while the latter has been introduced by Gayley (1995) in replacement of the initial K-factor of Castor et al. (1975) that was more correlated with α. Q is the quality factor corresponding to the coupling of radiation with the resonant spectral lines. The values of α and Q are computed from the opacity profiles of atomic lines and given for different stellar temperatures, surface gravity and metallicities. ρ refers to the mass density of the flow that goes as $r^{-2}v^{-1}$ in this spherically symmetric framework. The velocity gradient in the last factor originates from the aforementioned Doppler shifting.

The hydrodynamical effects are decisive for wind launching since they set the existence of a critical solution passing through a sonic point (Parker 1958). The thermodynamical conditions set the position of this sonic point and, by then, the global properties of the outflow (e.g. the mass-loss rate and the terminal speed). That being said, above the sonic surface (where the flow becomes supersonic), the dynamics of the flow is essentially ballistic. Furthermore, we aim at reproducing the expected velocity profile to investigate in more detail how it behaves in a SGXB but not at accurately modelling the wind launching in a self-consistent and physical way. The latter would require a proper hydrodynamical treatment to locate precisely the sonic point in each direction (in the three-dimensional framework of SGXB). This approach has already been carried out successfully for SGXB (Blondin et al. 1990; Manousakis & Walter 2015) but is too computationally time-demanding to be compatible with the comprehensive parameters space exploration we undertake. Besides, it yields sonic surfaces close from the stellar surface compared to the orbital scales we are concerned with. Consequently, we rely on a representation of the wind launching where the mass-loss rate is set by a formula derived from full hydrodynamical investigations (see Section 4.3) while the sonic surface is forced to the stellar surface, an approach that has already given fruitful results on the wind dynamics in SGXB (Ducci et al. 2009). The latter assumption prevents us from drawing any conclusion on the precise nature of the critical solution or the behaviour of the flow in the vicinity of the sonic surface but does enable us to empirically reproduce velocity profiles similar to the physical ones (see Fig. 1). The matching is not exact because contrary to the physically determined solutions (dashed lines), we do not solve the hydrodynamical equations. However, our aim is to explore the variety of behaviour of winds with realistic velocity profiles and mass-loss rates in SGXB, not to characterize the critical outflowing solution. To this extent, the solutions we compute (solid lines) are good enough and fast to compute since they only require a ballistic treatment (see Section 3.2).

In anticipation of the numerical integration of the full problem, no longer analytically solvable, we tested the integrator described in Section 3.2 on equation (A2). Fig. 1 illustrates the computed velocity profiles (red solid line) for a representative case and compares it to the analytical profile (A4) (red dashed line) reminded in Appendix A. Notice that this velocity profile is a specific case of the more phenomenological β-laws profiles fitted to the data with v_∞ and a free exponent, β, not necessarily 1/2 like above. The numerically derived velocity profiles and terminal velocities match

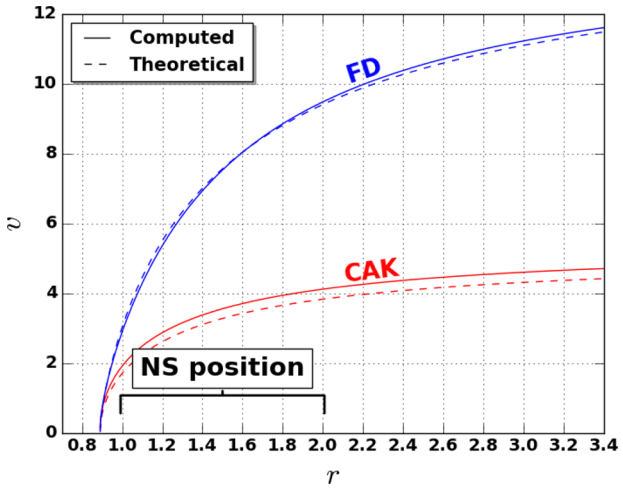

Figure 1. Typical velocity profile for an isolated star (in the arbitrary units system of Section 2.2) in the bedrock CAK model (red) and in the case where the finite disc effect has been included (blue). The red and blue dashed lines are the corresponding theoretical profiles given, respectively, by equations (A4) and (2).

the analytical ones within 10 per cent, a precision good enough to investigate forward the modified CAK model described below.

2.1.2 *Relaxing the finite cone angle assumption*

Since the compact object lies generally within a couple of stellar radii from the star centre in a SGXB and the accretion will critically depend on the velocity of the wind as it passes close to it, the initial phase of acceleration of the wind must be accurately modelled. An improvement on the theory described above in the vicinity of the launching surface is to consider the star no longer as a point source but as an extended emission region and integrate over all the incoming directions of the photons (Friend & Abbott 1986; Pauldrach, Puls & Kudritzki 1986; Kudritzki et al. 1989). Accounting for the finite size of the disc translates into an additional dimensionless factor D in equation (1) whose expression can be found in Appendix B. Accounting for this effect has two effects on the issued velocity profile. First, the exponent in the expression of the velocity profile rises, in the configurations we considered up to approximately 0.7, making the profile smoother. It is consistent with observations (Villata 1992) and sophisticated semi-analytical computation of modified CAK-wind profiles (Pauldrach et al. 1986; Villata 1992; Müller & Vink 2008; Araya, Curé & Cidale 2014), though on the lower end of the range. Second, the terminal speeds obtained are larger. Following the suggestions of recent state-of-the-art hydrodynamical simulations (Müller & Vink 2008; Noebauer & Sim 2015) and of analytical studies (Pauldrach et al. 1986; Kudritzki et al. 1989) about the terminal speeds, we compared our results to the following velocity profile:

$$v(r) = v_\infty \left(1 - \frac{R_*}{r}\right)^{0.7} \quad \text{with} \quad v_\infty \sim 2.5 v_{\rm esc} \frac{\alpha}{1-\alpha}, \qquad (2)$$

where the factor 2.5 holds for effective stellar temperatures beyond 21 000 K (Vink, Koter & Lamers 1999). Notice that this law leads to generally higher terminal speeds than the one suggested by Friend & Abbott (1986) but to similar values than the observed ones for class I luminosity stars (see table 3 of Groenewegen et al. 1989), if one considers $\alpha \sim 0.55$. Once again, we used a numerical integrator to compute the velocity profile and compared it to the profile above

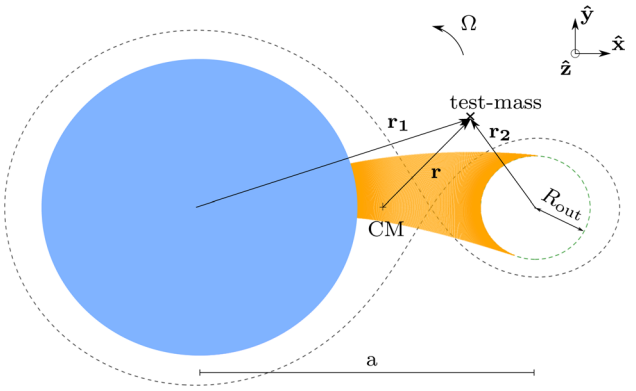

Figure 2. Orbital slice of the SGXB configuration we consider with, in blue, the supergiant stellar companion and on the right, the compact object. The eight-shaped black dotted line is the Roche surface passing through the first Lagrangian point and the orange lines are the computed streamlines that enters the vicinity of the compact object. The latter, in dashed green, is defined by its radius $R_{\rm out}$ as specified in Section 3.1. a is the orbital separation.

in Fig. 1. The numerically derived velocity profiles and terminal velocities match the theoretical values within a few per cents.

2.2 Scale invariant expression of the wind motion in a Roche potential

SGXB feature low-eccentricity orbits compared to the other classes of HMXB: we assume the system to be fully circularized, and the stellar spin to be synchronized (Claret & Gimenez 1997; Van Eylen, Winn & Albrecht 2016). We now set ourselves in the frame corotating at the orbital period,[2] with the centre of mass (CM) at the origin and use subscript 1 (respectively 2) to refer to the star (respectively to the compact object), as described in Fig. 2. Let us approximate the ratio of the stellar Roche lobe to the orbital separation with the function $\mathcal{E}$ of the mass ratio $q = M_1/M_2$ given by Eggleton (1983).

The dynamics of the supersonic flow at the orbital scale is dominated by the gravitational field of the star corrected for the continuous radiative pressure on free electrons,[3] the gravitational field of the compact object, the non-inertial forces (centrifugal and Coriolis) and the aforementioned radiatively driven wind acceleration applied to a test-mass. Because SGXB exhibit large mass ratios and because the typical speeds of radiatively driven winds quickly exceed the orbital speeds in SGXB, we make the following assumptions concerning the latter acceleration term.

(i) The steady state continuity equation departs little from its spherical expression: the product of the wind mass density by the radial velocity still evolves with the inverse of the distance to the star squared.

(ii) The properties of the sonic surface remain unchanged, set by the stellar parameters only (neither by the orbit nor by the accretion on to the compact object). The sonic surface is still spherical and coincides with the stellar surface.

(iii) The streamlines depart little enough from their initially radial direction to be able to neglect the influence of the non-radial velocity

[2] And so do all the velocities we refer to in this paper.

[3] Using the Eddington parameter Γ defined as the ratio of the stellar luminosity by its Eddington luminosity.

gradient in the line acceleration term compared to the other terms. For the same reason, we also neglect the non-radial components of the line acceleration that could arise.

In the ballistic framework, we consider the acceleration of a pressureless particle of fluid assimilated to a test-mass. The radiative acceleration term is adapted accordingly, using the isotropic steady state continuity equation aforementioned. So as to reduce the number of shape parameters to its very minimum and to explore the parameters space efficiently, we use the stellar Roche lobe radius $R_{\mathrm{R},1}$, the mass of the compact object M_2 and $GM_2/R_{\mathrm{R},1}^2$ as normalization quantities for length, mass and acceleration, respectively. The other scales are deduced by the simplest combinations of the scales above, without any additional dimensionless factor. Using the variables introduced in Fig. 2, we write $v_1 = \boldsymbol{v}\cdot(\boldsymbol{r_1}/r_1)$ the radial velocity of the test-mass projected on to the radial unity vector from the star. Then, we get the following dimensionless ballistic equation of motion of a radiatively driven wind in a SGXB effective Roche potential:

$$\frac{\mathrm{d}\boldsymbol{v}}{\mathrm{d}t} = -\left[\frac{q(1-\Gamma)}{r_1^3} - \aleph\cdot D\left(r_1, \frac{\mathrm{d}v_1}{\mathrm{d}r_1}; \alpha, f\right)\frac{v_1^\alpha}{r_1^{3-2\alpha}}\left(\frac{\mathrm{d}v_1}{\mathrm{d}r_1}\right)^\alpha\right]\boldsymbol{r}_1 - \frac{1}{r_2^3}\boldsymbol{r}_2 + (1+q)\mathcal{E}^2\boldsymbol{r}_\perp - 2\mathcal{E}^{3/2}\sqrt{1+q}\cdot\hat{\boldsymbol{z}}\wedge\tilde{\boldsymbol{v}}, \quad (3)$$

with $f = R_1/R_{\mathrm{R},1}$ the filling factor (where R_1 is the stellar radius), $\boldsymbol{r}_\perp$ the projection of $\boldsymbol{r}$ on the orbital plane and $\aleph$ a dimensionless quantity whose expression is set by the hydrodynamical requirement of the critical solution:

$$\aleph = \frac{1+\alpha}{\alpha}\left[\frac{\alpha}{1-\alpha}q(1-\Gamma)\right]^{1-\alpha}, \quad (4)$$

with the $1+\alpha$ factor to account for the finite cone angle effect. Forcing $\aleph$ to this value is the key to obtain empirical ballistic solution in relative agreement with the real critical solution (whose derivation requires a proper hydrodynamical treatment but is not the purpose of the present paper): if it is lower, the flow cannot take off and if it is larger, we depart more and more from the critical solution. Despite the apparent cumbersomeness of equation (3), the shape of the solutions depends only on four degrees of freedom: the filling factor f, the mass ratio q, the α force multiplier and the Eddington parameter Γ.

3 NUMERICAL PROCESS

3.1 The modified accretion radius

As visible in Fig. 1, the neutron star typically lies within the acceleration zone of the wind. This specific feature of SGXB compared to symbiotic binaries makes the accretion properties of the system possibly very sensitive to the ratio of the orbital separation to the characteristic acceleration length scale of the wind (Abate et al. 2013). One way to evaluate the amplitude of this accretion is to compute the accretion radius from the classical Bondi–Hoyle–Lyttleton (BHL) framework (Hoyle & Lyttleton 1939; Bondi & Hoyle 1944; Edgar 2004, for a review): for a planar flow with a relative supersonic velocity at infinity $v_\bullet$ with respect to a body of mass M_2, the accretion radius is given by $R_{\mathrm{acc}} = (2GM_2)/v_\bullet^2$. It is the critical impact parameter below which matter is likely to be accreted. Concerning $v_\bullet$, we get it by computing the velocity reached by a test-mass once it reaches the position of the compact object, but without the gravitational term of the neutron star in equation (3). Given the typical values of $v_\bullet$ ($\sim$1000 km s^{-1}), the flow is expected to be supersonic from the stellar surface to the vicinity of the compact object. Numerical simulations of BHL accretion show that the flow remains supersonic around the accretor beyond a few R_{acc} (El Mellah & Casse 2015). We then define an extended accretion sphere of radius $R_{\mathrm{out}} = 8R_{\mathrm{acc}}$ around the accretor where we stop our ballistic simulations. Within this sphere, a proper hydrodynamical treatment is compulsory, in particular in the wake of the accretor, and will be carried on in an upcoming paper. From now on, we refer to R_{out} and the sphere it defines as the 'extended' accretion radius and sphere.

3.2 Numerical implementation

To solve the equation of motion (3), we applied a fourth order Runge–Kutta scheme on test-masses starting at the surface of the star with a zero velocity. To initiate the wind and compute the radial velocity gradient in equations (1) and (B1), we force the first step with radial and velocity steps small compared to the stellar radius and to the velocities computed afterwards. Because $\aleph$ is forced to its critical value, the computed velocity profile depends little on those arbitrary steps. Once the integration brought the test-mass trajectory to intercept (respectively miss) the extended accretion sphere around the compact object, its position and velocity on the sphere are saved (respectively discarded). To better resolve the borders and improve the statistical significance of our computation of the characteristic quantities of the inflow within the extended accretion sphere, we then refine the initial positions at the surface of the star that were selected and repeat the integration until we are left with a few 10 000 selected arrival points to process. Some of the streamlines susceptible to be accreted have been represented in orange in Fig. 2 in a fiducial case.

Concerning the primitive quantities at the extended accretion sphere, we save the velocity and positions of the test-masses when they reach it. Since our model is purely ballistic, we cannot access the density directly but we can get the divergence of the streamlines by monitoring the evolution of the surface elements delimited by the four closest streamlines at the departure and at the arrival. Once a physical scale has been chosen, we can then deduce from this value the density corresponding to each streamline on the extended accretion sphere. An angular resampling of those primitive quantities (mass density and velocity) on pre-defined meshes provides us with physically motivated outer boundary conditions for upcoming hydrodynamical simulations on the fate of this inflow within the extended accretion sphere.

3.3 Parameters and visualization

We sample the four shape parameters accordingly to the values expected in a neutron star hosting SGXB.

(i) α is either 0.45, 0.50, 0.55 or 0.65. If the latter value is more suited for early supergiant O-type stars, the three first ones correspond to the values calculated by Shimada et al. (1994) and Puls, Springmann & Lennon (2000) for early B/late O supergiant stars with solar metallicity. The value of α depends mostly on the effective stellar temperature T and the decimal logarithm of the surface gravity, $\log(g)$.

(ii) Γ, the Eddington parameter. For OB supergiants, we expect it to be below 30 per cent, by opposition to Wolf–Rayet stars, luminous blue variables or hypergiant stars (like the donor in GX 301−2) that

can go beyond. We take 10, 20 and 30 per cent as the three possible values.

(iii) q, the mass ratio. We ran simulations for 12 integer values of q ranging between 7 and 18.

(iv) f, the filling factor. We picked up 10 values non-regularly spaced between 50 and 99 per cent.

To access physical outputs (such as the stellar radius or the mass accretion rate on to the compact object), we also need user-specified scale parameters: the orbital period, the mass of the compact object and the Q force multiplier (to compute the physical mass-loss rate of the star). According to Shimada et al. (1994), Q lies in a narrow range around 900 for early-type B supergiant stars with effective temperatures above the bi-stability threshold (∼20 kK; Vink et al. 1999) and below 30 kK. Puls et al. (2000) obtain somewhat larger values, above 1000. Based on the SPYRE library for PYTHON developed by Hajari (2015), we developed a visualization interface, available on demand, to conveniently explore the outputs in this 4+3 comprehensive parameters space.

4 STRUCTURE AND PROPERTIES OF THE FLOW AT THE ORBITAL SCALE

Based on the model presented in Section 2.2 and using the methodology described in Section 3, we analyse the evolution of the structure of the flow at the orbital scale with the fundamental parameters we exhibited previously. In particular, we quantify the beaming of the stellar wind along a stream between the star and its compact companion (Section 4.1), we evaluate the fraction of the wind accreted (Section 4.2) and we deduce the permanent X-ray luminosity (Section 4.3).

4.1 Structure of the accretion flow

We now try to quantify what we mean by 'wind' accretion. The usual smoking gun to qualify an accretion mechanism of wind accretion in a binary system is to observe an underflowing star with an accreting companion. However, it does not tell us much about the actual structure of the flow. Indeed, a wind that would not be fast enough compared to the orbital velocity once it reaches the critical Roche surface would result in a highly collimated flow, mimicking the stream one usually associates with Roche lobe overflow (RLOF; Nagae et al. 2005; Mohamed 2010). RLOF tells us something about the filling factor while wind accretion refers to the structure of the flow, not necessarily incompatible with RLOF. Thus, we choose to term 'wind' or 'stream' an accretion flow depending on the relative size of the extended accretion sphere $R_{\rm out}$, where the shock is expected to develop, with respect to the size of the Roche lobe of the compact object $R_{\rm R,\,2}$. When the wind is slow, the former becomes of the order or even larger than the latter and the whole orbital scale requires a proper hydrodynamical treatment.

To evaluate how slow the wind must be to be in such a configuration, we plotted in Fig. 3 the evolution of the ratio of the aforementioned length scales compared to the ratio of $v_\bullet$ to the orbital speed. As expected, $R_{\rm out}/R_{\rm R,\,2}$ follows $(v_\bullet/a\Omega)^{-2}$. The normalization depends on the mass ratio but varies little for values of q suitable to SGXB. With this figure, we notice that, even in configurations where the filling factor is close to one, a high velocity flow (a wind) is expected for efficient wind acceleration (i.e. $\alpha > 0.55$), for any Eddington factor below 30 per cent. It is a typical situation where RLOF cohabits with wind accretion. On the other hand, even for a filling factor as low as 90 per cent, one can get a

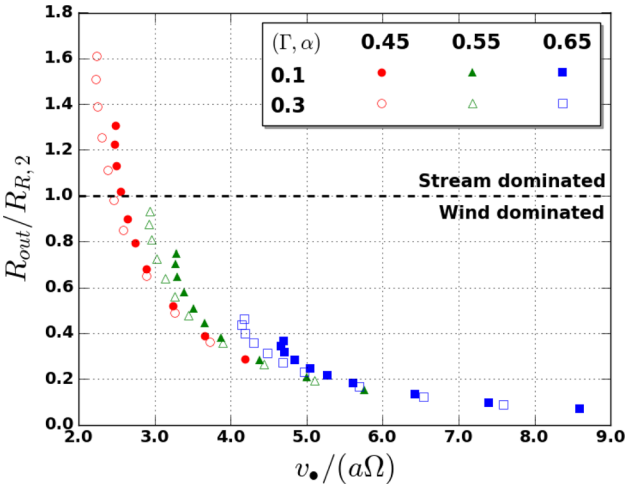

Figure 3. Ratio of the extended accretion radius to the size of the compact object Roche lobe as a function of the ratio of the velocity at the orbital separation to the orbital speed. For each of the six curves, from upper left to lower right, we used values of (f, q) along the line going from (0.99, 8) to (0.5, 17) in Fig. 4 so as to probe the largest range of $R_{\rm out}/R_{\rm R,2}$.

stream-dominated flow for $\alpha = 0.45$, intermediate mass ratios and Eddington factors of 30 per cent. We observe that lower values of Γ, i.e. of the dimensionless luminosity, favour a wind-dominated flow.

An important conclusion to draw from Fig. 3 is also that, as far as the structure of the accretion flow is concerned, the ratio $v_\bullet/a\Omega$ is a reliable tracer to evaluate the beaming of the wind towards the accretor along a stream, much more reliable than the filling factor that only plays a secondary role here. We find a threshold of the order of 2.5 to distinguish between a stream (below) and a wind (above) dominated accretion flow.

4.2 Fraction of wind captured

First, we compute β^+, the fraction of stellar wind entering the extended accretion sphere (green dashed delimited region in Fig. 2). It corresponds to an upper limit on the actual fraction of the wind accreted and thus involved in the subsequent emission of X-rays, β. Concerning the latter, we cannot make any definitive measure without three-dimensional hydrodynamical simulations of the evolution of the flow within the extended accretion sphere. However, an indirect measure of β can be obtained using the results of El Mellah & Casse (2015). It showed that for Mach numbers of the incoming flow above 3, approximately 1 per cent of the flow entering the extended accretion sphere is doomed to be accreted, hence $\beta \sim \beta^+/100$.

The evolution of β follows the one of the angular size of the extended accretion sphere seen from the stellar surface, which explains its rise with the filling factor. However, its dependence on the mass ratio at a given filling factor (and Eddington parameter and α force multiplier) is not obvious. Indeed, on one hand the terminal speed is proportional to the escape velocity that rises with q and on the other hand, relative distance between the stellar surface and the compact object drops, giving the wind less room to accelerate. Thus, it is not possible to conclude a priori about the evolution of β with q and numerical computation was indeed required to obtain this tendency: for any filling factor, rising the mass ratio from 7

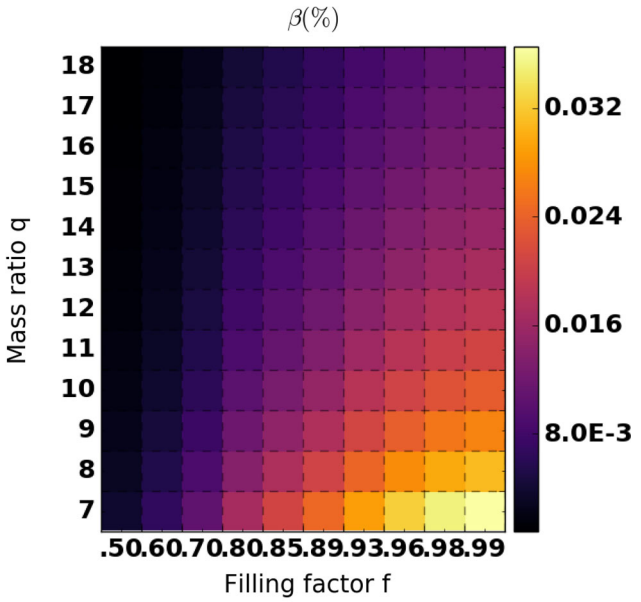

Figure 4. Measured fraction of wind accreted for $\alpha = 0.45$ and $\Gamma = 0.2$ as a function of the filling factor and the mass ratio.

to 18 leads to a drop in the fraction of wind accreted by a factor of 3. As α rises, the wind acceleration gets more efficient and the terminal speed is higher, making the speed at the orbital separation larger and the computed accretion radius smaller. Thus, β drops by approximately an order of magnitude as α rises from 0.45 to 0.65. Although the fraction of wind being accreted depends on α, it is worth noticing that it does not depend on the Q force multiplier: whatever its value, the velocity profile remains unchanged. Eventually, for the influence of Γ, a rise from 10 to 30 per cent only results in a rise of a factor less than 2 for β, but it will play a more important role once its influence on the mass outflow is taken into account.

4.3 Physical mass accretion rate and X-ray luminosity

We now go on by analysing a scale-dependent decisive output, the physical mass accretion rate and the associated X-ray luminosity L_X. Interestingly enough, Fig. 4 shows that, for a fixed mass of the compact object, the fraction of wind accreted decreases when the mass of the supergiant star rises. However, this statement, along with all the ones made in the previous section, concerns only the fraction of wind that is accreted, not the actual physical mass accretion rate: since a larger stellar mass also means a larger absolute mass-loss rate, the evolution of the X-ray luminosity with q remains unknown.

To compute the physical mass accretion rate, we first need an estimation of the stellar mass-loss rate $\dot{M}_1$. Although our empirical treatment of the launching of the wind reproduces the expected velocity profiles, it prohibits any measure of the mass outflow in our simulations and we need to rely on the results derived by more sophisticated hydrodynamical investigations (Kudritzki et al. 1989; Müller & Vink 2008; Noebauer & Sim 2015). Following their approach, the analytical expression of the CAK wind mass-loss rate can be obtained from the consideration described in Section 2.1.1 and Appendix A and, in particular, from the expression of the critical $\aleph$. Once reinjected in equation (A2) and after replacing the mass density ρ in equation (1) by $\dot{M}_1/4\pi r^2 v$ (continuity equation) and correcting for the finite cone angle effect (first factor below), we get:

$$\dot{M}_1 = \left(\frac{1}{1+\alpha}\right)^{\frac{1}{\alpha}} \frac{\alpha}{1-\alpha}\Gamma \left(\frac{\Gamma Q}{1-\Gamma}\right)^{\frac{1-\alpha}{\alpha}} \frac{L_{\rm Edd}}{c^2}, \tag{5}$$

where $L_{\rm Edd}$ is the Eddington luminosity of the star. This expression is strictly equivalent to equation (A.12) in Noebauer & Sim (2015) but written with the Q force multiplier introduced by Gayley (1995). Since we know the fraction β of the wind accreted, we have the physical mass accretion rate on the compact object. The corresponding X-ray luminosity is then computed for an accretor of compactness parameter representative of a neutron star (∼25 per cent).

Fig. 5 represents the evolution of the steady-state X-ray luminosity as a function of the four shape parameters. Given the restricted range of expected values for Q and M_2 and the weak dependency of L_X (via $\dot{M}_1$) on them, we chose to highlight the dependence of the X-ray luminosity on the dimensionless parameters.

The main conclusion to draw from this figure is that the impact of the α force multiplier on the mass accretion rate is so important that one cannot reach the observed X-ray luminosities for α significantly larger than 0.55, whatever the other parameters. Because the ionizing X-ray feedback will be inefficient in low X-ray luminosities, we do not expect any inhibition of the wind acceleration in the direction of the accretor that would enhance the mass accretion rate (Ho & Arons 1987b). Consequently, we can affirm that there is a strong observational bias in favour of high-mass stars with a lower α force multiplier, typically early-B supergiant stars rather than O supergiant stars, in spite of the larger mass-loss rate of the latter. If there exists a population of SGXB with high α donor stars, only systems departing from the present model can be detected in permanent regime: Roche lobe overflowing systems such as Cen X-3 (Suchy et al. 2008) or systems where the wind is excessively inhomogeneous such as 4U 1700−37 (Boroson et al. 2003) for instance. Since α is also lower for lower metallicity stars, the donors observed in SGXB have statistically lower metallicity than isolated stars of similar spectral type.

Eventually, we do insist on the fact that this parametrization alleviates the dependency of the X-ray luminosity on the orbital period. The key point is that, if the orbital period rises, β is not altered since it is a geometrical dimensionless quantity: physically, it means that the accretion radius $R_{\rm acc}$ rises in the same proportions as the orbital separation a. Also, changing the orbital period does not modify the stellar mass outflow[4] that finally makes the X-ray luminosity independent of the orbital period. As a consequence, we claim that any dependency of the observed X-ray luminosities on the orbital periods must be attributed either to a departure from the present framework or to an underneath correlation not taken into account, for instance between the Eddington factor Γ and the stellar radius, expected to be smaller for shorter period systems not undergoing RLOF: for stellar evolution reasons, the orbital separation is likely to be negatively correlated to the filling factor. In no case the orbital period could be considered as the main culprit for the X-ray luminosity, merely as a correlated quantity whose causal relation to the permanent X-ray luminosity must be traced back.

[4] At least for large mass ratios for which we supposed that the mass of the neutron star was too low compared to the stellar mass to alter the launching of the wind, essentially determined by the conditions at the sonic (here, stellar) surface.

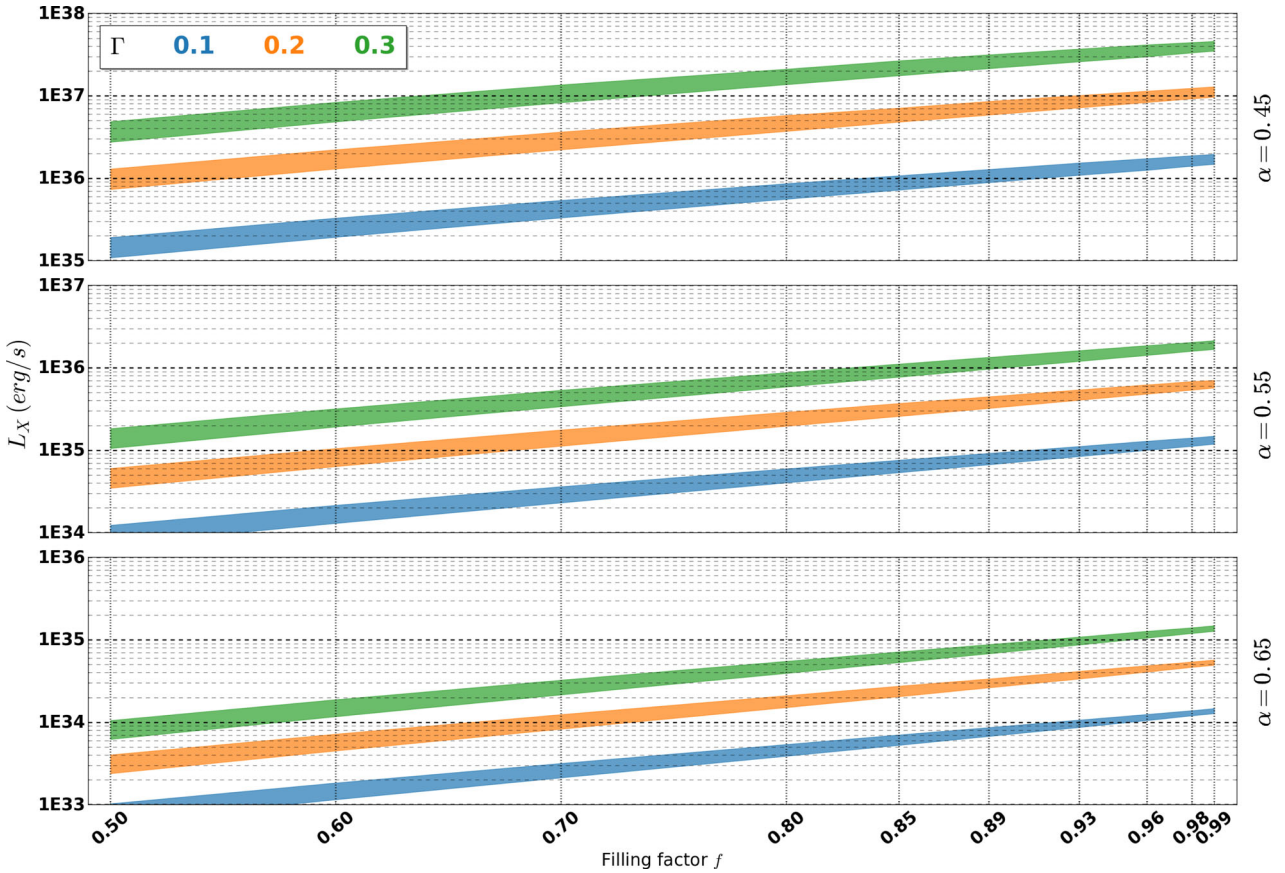

Figure 5. Representation of the permanent X-ray luminosity as a function of the filling factor f, for different α force multipliers (different panels) and Eddington factors Γ (different colours). The weaker dependence on the mass ratio, which ranges from 7 to 18, is represented by the thickness of each line (the lower end of each stripe being for larger mass ratios): since M_2 is set to 1.8 $M_\odot$ here, M_1 spans a realistic interval of 13–32 $M_\odot$. We numerically computed the accretion radius as described in Section 3.1 and sampled the filling factors denoted at the bottom. Those results are computed for an intermediate value of the Q force multiplier of 900. Changing the orbital period while keeping those quantities invariant does not modify those results.

4.4 Shearing of the accretion flow

The question of the angular momentum accretion rate within the extended accretion sphere and of its dependencies on the four shape and three scale parameters remains. Do the configurations favourable to large X-ray luminosities correspond to the ones likely to give birth to a disc around the accretor? To possibly form a disc-like structure around the accretor, the flow needs to gain enough angular momentum as it approaches the compact object. We computed for each configuration the circularization radius corresponding to the inflowing angular momentum within the extended accretion sphere. It correlates positively with the X-ray luminosity and traces the likelihood to form a wind capture disc. Compared to the accretion radius at its upper end, it shows that any disc-like structure would form within the shocked region while the accretion wake itself will be only slightly bent, with a higher curvature for slower winds. Because substantial instabilities could take place within the shocked region around the accretor (for instance an axisymmetric analogue of the spherical resonant advective-acoustic cycle discovered by Foglizzo & Tagger 2000), the features of the redistribution of angular momentum as the gas is accreted remain to be investigated.

Compared to the size of the accreting neutron star, the circularization radius is larger by 2–3 orders of magnitude for moderately fast winds (typically $\alpha \lesssim 0.55$). It is large enough to immunize a putative disc against premature truncation by the magnetosphere, provided the angular momentum of the flow is not significantly depleted within the extended accretion sphere.

5 DISCUSSION AND SUMMARY

We used a synthetic model to describe the physics at stake in SGXB and couple the different mechanisms. We showed that the scale-invariant properties can be fully derived from four dimensionless numbers:

(i) the mass ratio between the supergiant OB star and the neutron star;
(ii) the stellar filling factor;
(iii) the α force multiplier associated with the launching of the wind;
(iv) the ratio of the stellar luminosity to its Eddington luminosity.

Those parameters can be estimated using observables such as the orbital period, the X-ray persistent luminosity, the stellar temperature T or the stellar surface gravity $\log_{10}(g_{\rm CGS})$ (hereafter $\log(g)$). Coupled to information on α and Q from stellar atmospheric models, they can provide a first comprehensive and self-consistent overview of a given SGXB comparatively with others. For instance, spectroscopic inquiries of the pressure-broadened Balmer and He II lines coupled to stellar atmospheres codes set constrains on $\log(g)$ and on T (Clark et al. 2002). Once corrected for radiative pressure (Sander

Table 1. Sets of self-consistent fundamental parameters associated with each system. No uncertainty is specified because the systematic effects dominate and are discussed in the text in more details. Those values serve to compare the three systems to each other, not to specify precisely the parameters of each system. They indicate a trend, not a state.

	Vela X-1	XTE J1855−026	IGR J18027−2016
q	12	14	11
f	95 per cent	89 per cent	98 per cent
α	0.50	0.50	0.45
Γ	$\gtrsim$20 per cent	30 per cent	10 per cent
P (d)	8.96	6.07	4.47
M_2 ($M_\odot$)	2	$\lesssim$2	1.5
Q	900	900	1100

et al. 2015), $\log(g)$ features few dependencies such as it narrows the range of filling factors possible:

$$f \sim \underbrace{\frac{0.32q^{1/2}}{\mathcal{E}(q)(1+q)^{1/3}}}_{78\text{ per cent}\rightarrow 82\text{ per cent}} \left(\frac{M_2}{2\,M_\odot}\right)^{\frac{1}{6}} \left(\frac{9\,\mathrm{d}}{P}\right)^{\frac{2}{3}} 10^{\frac{3-\log(g)}{2}}, \quad (6)$$

where the bracket evaluates the factor it embraces as q goes from 7 to 18. The dependence on the mass of the compact object is also weak, accounting for a few per cent only for a neutron star. Since the orbital period is precisely known (when measured), we can affirm that $\log(g)$ is a direct measure of the filling factor. Its precise knowledge (i.e. with a precision of at most a few per cents), along with the orbital period, is a precious and sufficient asset to enclose the value of the filling factor in a ∼10–20 per cent precision range. In parallel, we deduce the Eddington factor from the prior of T and $\log(g)$, using a Thomson scattering opacity from Kudritzki et al. (1989) with two electrons provided per helium nucleus and a fraction of helium with respect to hydrogen of 20 per cent:

$$\Gamma \sim 0.23 \left(\frac{T}{25\,\mathrm{kK}}\right)^4 10^{3-\log(g)}. \quad (7)$$

The consistency of the parameters derived in this approach with the permanent X-ray luminosity and possibly additional observables in eclipsing SGXB brings additional support to this model. Using the measured orbital periods (Quaintrell et al. 2003; Mason et al. 2011; Falanga et al. 2015; Walter et al. 2015; Gimenez-Garcia et al. 2016), we worked out the most consistent fundamental parameters (see Table 1) and deduced the corresponding orbital, stellar, wind and accretion parameters (terminal wind speed, β-exponent of the velocity profile, stellar mass, permanent mass accretion rate, etc.) for three classical SGXB hosting an eclipsing neutron star and where the donor is of early-B type (B0-1): Vela X-1, XTE J1855−026 and IGR J18027−2016 (also known as SAX 1802.7−2017). The results turn out to follow the observational trends from a system to another, which indicates that they fit this framework of ballistic steady-state radiatively driven wind in a Roche potential.

We showed that the transition from a stream-dominated flow, reminiscent from RLOF, to a wind-dominated flow can be handled continuously and characterized with a threshold on the ratio of the speed of the wind at the orbital separation to the orbital speed. The accurate wind acceleration mechanism we rely on provides a realistic estimation of the kinetic energy the flow acquired when it reaches the vicinity of the accretor. The subsequent accretion amplitudes display a significant enhancement that is enough to reproduce the observed persistent X-ray luminosities in SGXB in general and in particular for SGXB where the donor star is of early-B spectral type such as the three systems aforementioned. If the shearing of the flow is not large enough to produce a disc before the bow shock ahead the neutron star (El Mellah & Casse 2015), the circularization radii we computed do leave the door opened to a wind-capture disc within the shocked region, provided the mass ratio is low enough, the wind acceleration inefficient enough (i.e. α low) and the filling factor and the Eddington parameter are large enough. Most importantly, we explicited the sets of parameters of interest and the associated outer boundary conditions for three-dimensional hydrodynamic simulation within the extended accretion sphere.

We did not consider the inhomogeneities and internal shocks in our model (Owocki, Castor & Rybicki 1988; Owocki 1991; Sundqvist & Owocki 2015). However, radiatively driven winds are notoriously unstable and form clumps with overdensities of a factor of 100 or so (Ducci et al. 2009), in particular within a couple of stellar radii from the star (Negueruela et al. 2008), a region where the accretor lies in those close-in HMXB. Accounting for clumpiness might not just be a question of time variability and spatial distribution of the wind but might also induce a proper shift of the mean wind density and, by then, of the X-ray luminosity. This point could also help to retrieve the observed persistent X-ray luminosities without having to assume low values of α.

ACKNOWLEDGEMENTS

IEM wants to thank Allard Jan Van Marle and Jon Sundqvist for insightful discussions on the physical mechanism responsible for winds of massive stars and the numerical methods available to implement it. IEM also thanks Jérôme Rodriguez and Alexis Coleiro for their precious suggestions of relevant systems susceptible to be well described by the model presented in this paper. Maïca Clavel also brought fruitful comments to evaluate the X-ray absorption of those three systems. Last but not least, significant improvements have been made possible thanks to the dedicated reviewing of the anonymous referee. May he/she be thanked for his/her insightful comments.

REFERENCES

Abate C., Pols O. R., Izzard R. G., Mohamed S. S., de Mink S. E., 2013, A&A, 552, A26
Araya I., Curé M., Cidale L. S., 2014, ApJ, 795, 81
Blondin J. M., Kallman T., Fryxell B., Taam R. E., 1990, ApJ, 356, 591
Bondi H., Hoyle F., 1944, MNRAS, 104, 273
Boroson B., Vrtilek S., Kallman T., Corcoran M., 2003, ApJ, 592, 516
Castor J. I., Abbott D. C., Klein R. I., 1975, ApJ, 195, 157
Chaty S., 2011, in Schmidtobreick L., Schreiber M. R., Tappert C., eds, ASP Conf. Ser. Vol. 447, Evolution of Compact Binaries. Astron. Soc. Pac., San Francisco, p. 29
Claret A., Gimenez G., 1997, A&A, 318, 187
Clark J. S., Goodwin S. P., Crowther P. A., Kaper L., Fairbairn M., Langer N., Brocksopp C., 2002, A&A, 392, 909
Coleiro A., Chaty S., 2013, ApJ, 764, 185
Crowther P. A., Lennon D. J., Walborn N. R., 2006, A&A, 446, 279
de Val-Borro M., Karovska M., Sasselov D., 2009, ApJ, 700, 1148
Ducci L., Sidoli L., Mereghetti S., Paizis A., Romano P., 2009, MNRAS, 398, 2152
Edgar R. G., 2004, New Astron. Rev., 48, 843
Eggleton P. P., 1983, ApJ, 268, 368
El Mellah I., Casse F., 2015, MNRAS, 454, 2657
Falanga M., Bozzo E., Lutovinov A., Bonnet-Bidaud J. M., Fetisova Y., Puls J., 2015, A&A, 577, A130
Filliatre P., Chaty S., 2004, ApJ, 616, 469
Foglizzo T., Tagger M., 2000, A&A, 363, 174

Foulkes S. B., Haswell C. A., Murray J. R., 2006, MNRAS, 366, 1399
Friend D. B. D., Abbott D. C. D., 1986, ApJ, 311, 701
Gayley K. G., 1995, ApJ, 454, 410
Gimenez-Garcia A. et al., 2016, A&A, 591, A26
Groenewegen M. A. T., Lamers H. J. G. L. M., Pauldrach A. W. A., 1989, A&A, 221, 78
Ho C., Arons J., 1987a, ApJ, 316, 283
Ho C., Arons J., 1987b, ApJ, 321, 404
Hoyle F., Lyttleton R. A., 1939, Math. Proc. Cambridge Philos. Soc., 35, 405
Huarte-Espinosa M., Carroll-Nellenback J., Nordhaus J., Frank A., Blackman E. G., 2013, MNRAS, 433, 295
Illarionov A. F., Sunyaev R. A., 1975, A&A, 39, 185
Jahanara B., Mitsumoto M., Oka K., Matsuda T., Hachisu I., Boffin H. M. J., 2005, A&A, 441, 589
Kudritzki R. P., Puls J., 2000, ARA&A, 38, 613
Kudritzki R. P., Pauldrach A., Puls J., Abbott D. C., 1989, A&A, 219, 205
Lamers H. J. G. L. M., Cassinelli J. P., 1999, Introduction to Stellar Winds. Cambridge Univ. Press, Cambridge
Lucy L. B., Solomon P. M., 1970, ApJ, 159, 879
MacGregor K. B., Hartmann L., Raymond J. C., 1979, ApJ, 231, 514
Manousakis A., Walter R., 2015, A&A, 575, A58
Mason A. B., Norton A. J., Clark J. S., Negueruela I., Roche P., 2011, A&A, 532, A124
Mohamed S., 2010, PhD thesis, St Edmund Hall, Univ. Oxford
Mohamed S., Podsiadlowski P., 2007, preprint (arxiv:e-prints)
Müller P. E., Vink J. S., 2008, A&A, 492, 493
Nagae T., Oka K., Matsuda T., Fujiwara H., Hachisu I., Boffin H. M. J., 2005, A&A, 441, 589
Negueruela I., Casares J., Verrecchia F., Blay P., Israel G., Covino S., 2008, Astron. Telegram, 1876, 1
Noebauer U. M., Sim S. A., 2015, MNRAS, 453, 3120
Owocki S. P., 1991, in van der Hucht K. A., Hidayat B., eds, Proc. IAU Symp. 143, Wolf-Rayet Stars and Interrelations with Other Massive Stars in Galaxies. Kluwer, Dordrecht, p. 155
Owocki S. P., Rybicki G. B., 1984, ApJ, 284, 337
Owocki S. P., Rybicki G. B., 1985, ApJ, 299, 265
Owocki S. P., Castor J. I., Rybicki G. B., 1988, ApJ, 335, 914
Parker E. N., 1958, ApJ, 128, 664
Pauldrach A., Puls J., Kudritzki R. P., 1986, A&A, 164, 86
Puls J., Springmann U., Lennon M., 2000, A&AS, 141, 23
Puls J., Vink J. S., Najarro F., 2008, A&AR, 16, 209
Quaintrell H., Norton A. J., Ash T. D. C., Roche P., Willems B., Bedding T. R., Baldry I. K., Fender R. P., 2003, A&A, 401, 313
Sander A., Shenar T., Hainich R., Gímenez-García A., Todt H., Hamann W.-R., 2015, A&A, 577, A13
Shakura N., Postnov K., Hjalmarsdotter L., 2013, MNRAS, 428, 670
Shakura N. I., Postnov K. A., Kochetkova A. Y., Hjalmarsdotter L., Sidoli L., Paizis A., 2015, Astron. Rep., 59, 18
Shimada M. R., Ito M., Hirata B., Horaguchi T., 1994, in Balona L. A., Henrichs H. F., Le Contel J. M., eds, Proc. IAU Symp. 162, Pulsation; Rotation; and Mass Loss in Early-Type Stars. Kluwer, Dordrecht, p. 487
Suchy S. et al., 2008, ApJ, 675, 1487
Sundqvist J. O., Owocki S. P., 2015, MNRAS, 453, 3428
Theuns T., Jorissen A., 1993, MNRAS, 265, 946
Theuns T., Boffin H. M. J., Jorissen A., 1996, MNRAS, 280, 1264
Van Eylen V., Winn J. N., Albrecht S., 2016, ApJ, 824, 15
Villata M., 1992, A&A, 257, 677
Vink J. S., de Koter A., Lamers H. J. G. L. M., 1999, A&A, 350, 181
Walter R., Lutovinov A. A., Bozzo E., Tsygankov S. S., 2015, A&AR, 23, 2

APPENDIX A: SOLUTION OF THE DIMENSIONLESS CAK PROBLEM

In spite of the apparent cumbersome aspect of the most simple form of the CAK wind in equation (1), the only parameter that sets the shape of the flow is the α force multiplier. Indeed, with tildes referring to dimensionless quantities, equation (1) can be rewritten as

$$\tilde{g}_{\rm CAK} = \frac{1}{\tilde{r}^{2(1-\alpha)}} \left(\tilde{v} \frac{{\rm d}\tilde{v}}{{\rm d}\tilde{r}} \right)^{\alpha}. \tag{A1}$$

Thus, the steady-state pressureless equation of motion of the flow is given by, once normalized with the relevant unit scales (see below),

$$v \frac{{\rm d}v}{{\rm d}r} = -\frac{1}{r^2} + \frac{\aleph_0}{r^{2(1-\alpha)}} \left(v \frac{{\rm d}v}{{\rm d}r} \right)^{\alpha}, \tag{A2}$$

where tildes have been omitted. The first term is the modified gravity (i.e. which includes the radiative pressure on free electrons) and $\aleph_0$ is a dimensionless quantity that engulfs the other variables. It can be shown (Lamers & Cassinelli 1999) that the value of $\aleph_0$ is not free, if we force the uniqueness of the solution. If we introduce G the gravitational constant, M_* the mass of the star, Γ its Eddington factor and V and R, two fiducial scaling quantities (respectively for velocities and lengths), $\aleph_0$ is given by

$$\aleph_0 = \frac{1}{\alpha} \left(\frac{\alpha}{1-\alpha} \right)^{1-\alpha} \left[\frac{GM_*(1-\Gamma)}{RV^2} \right]^{1-\alpha}. \tag{A3}$$

In the case of an isolated star, one can always choose R and V such as the term between brackets in equation (A3) is 1 and the equation of motion takes the form of equation (A2) that can be integrated to find the well-known analytical expression of the velocity profile. When the terminal speed v_∞, typically several times the effective escape velocity $v_{\rm esc} = \sqrt{[2GM_*(1-\Gamma)]/R_*}$, turns out to be large with respect to the initial speed at the stellar surface (typically smaller than the sound speed), we have

$$v(r) = v_\infty \sqrt{1 - \frac{R_*}{r}} \quad \text{with} \quad v_\infty = v_{\rm esc} \sqrt{\frac{\alpha}{1-\alpha}}. \tag{A4}$$

APPENDIX B: FINITE CONE ANGLE FACTOR

To relax the point-source assumption, one has to consider the following dimensionless factor D to account for the finite cone angle effect, i.e. the fact that photons not travelling radially can also be absorbed:

$$D(r, {\rm d}v/{\rm d}r; \alpha, R_*) = \frac{(1+\sigma)^{1+\alpha} - (1+\sigma\mu_{\rm C}^2)^{1+\alpha}}{(1+\alpha)(1-\mu_{\rm C}^2)\sigma(1+\sigma)^{\alpha}}, \tag{B1}$$

with R_* the stellar radius, r the distance to the stellar centre, $\sigma = ({\rm d}\log v/{\rm d}\log r) - 1$ and $\mu_{\rm C}^2 = 1 - (R_*/r)^2$. For $r \gg R_*$, one retrieves $D \sim 1$ but for $r \sim R_*$, D reaches its lowest value above the sonic surface, $D_0 = 1/(1+\alpha) < 1$, that rises the critical value of $\aleph_0$ (see Appendix A) required to make the launching possible (since otherwise, the CAK acceleration would no longer be large enough to overcome gravity).

This paper has been typeset from a TEX/LATEX file prepared by the author.